MP-End2End: Low Cost 3D analysis of Microplastics with DFF

Victor Sim[a,*], **Josiah Essiam**[a,1] **and Wang Ngai Ng**[a,1]

[a]Winchester College, College St, Winchester SO23 9NA

Abstract. Microplastics, formed by the breakdown of non-biodegradable plastic, pose a significant threat to aquatic ecosystems. To address this issue, accurate methods for quantifying microplastic concentrations are essential for informing policy and prosecuting offenders. Current detection methods, however, require expensive equipment and are often unreliable. We propose a new, cost-effective methodology that composites depth-from-focus techniques with few-shot classification. Unlike traditional methods that count and measure the size of microplastics, which can yield misleading results due to variability in particle shapes and densities, our approach will yield more accurate quantitative measures of microplastics on the environment. Additionally, qualitative analysis of the data can provide deeper insights into the physical and biological mechanisms driving microplastic ecosystem damage.

1 Introduction

Microplastic (defined as water-insoluble, solid polymer particles that are $\leq$5mm in size [3]) pollution has become an increasingly alarming issue. The number of microplastics in aquatic ecosystems are worrying: there are between 82 to 358 trillion microplastics in the world's oceans, weighing between 1.1 to 4.9 million tons.[4].

Microplastics (MP) have significant impact on marine ecosystems. According to Lee et al [12], "Microplastics ... move easily through the food chain and persist in the environment". Ingestion of MPs results in "physical and mechanical harm to marine organisms", causing "abnormalities in internal organs" and malnutrition due to "microplastic accumulation".Even exposure to MPs can cause harm: MPs "attach to the surface of skin, crust and ectoderm"[2] of small marine organisms.

Although microplastic pollution is a significant issue, there is a notable lack of accurate data. Lee et al [12] motivate their research by stating that "accurate statistics are unavailable regarding the sources of microplastics and the total amount of microplastics deposited in the land and sea" and "main sources of microplastics have not been clearly identified". A 2019 review paper on freshwater microplastic contamination [10] finds that the "level of quality assurance is varied" across existing studies.

The standard method for microplastic quantification is to use light microscopy. According to Hidalgo-Ruz et al. (2012), which reviewed 68 studies regarding microplastic identification and quantification, "In all reviewed studies, visual examination of the concentrated sample remains is an obligatory step. Careful visual sorting of residues is necessary to separate the plastics from other materials." Moreover, Primpke et al. (2020) states that "In many cases, light microscopy can be used without complex extraction methods, and researchers can be quickly and easily trained to visually identify MP.

However, the number of MP in a sample is commonly biased due to the difficulty in identifying non-obvious plastic particles from similar looking organic particles. More modern methods of MP classification have started adopting the use of machine learning for higher accuracy rates and efficiency. For example, Lorrenzo-Navarro et al. (2021) presents a "Deep learning approach for automatic counting and classification" that yields an impressive result: "A Jaccard index value of 0.8 is achieved in the experiments of particles segmentation and an accuracy of 98.11%". However, this method is unable to accurately quantify the amount of MPs in a sample as it relies on simply counting the number of MPs. Thus, important volume and mass information is lost in the process. As Hidalgo-Ruz et al. states, "The variable units in which abundance and mass of microplastics are reported become problematic when different studies are compared, even though units can be transformed in some cases".

To combat this, we present a novel method for the cost-effective and automated analysis of MPs in freshwater ecosystems. We improve the accuracy and quality of existing data by using depth-from-focus techniques to create 3D models of MPs. This is motivated by two insights.

Firstly, larger and more voluminous MPs break down into smaller MPs. If we only record the number of MPs, we may mistakenly identify MP types that are more prone to breaking down as being more prevalent. This could shift efforts away from addressing the primary sources of MP pollution, leading to ineffective mitigation.

Secondly, according to Barchiesi et al. [1], "The effects and risks of MPs correlate with three-dimensional (3D) properties, such as the volume and surface area of the biologically accessible fraction of the diverse particle mixtures as they occur in nature." 3D data is clearly significant in analysing the specific effects of MPs on ecosystems. For example, Ward et al. [19] find that "the extent of microplastic transport and deposition varied significantly by shape". Furthermore, they even find that "accurately modelling the shape of ... microplastic transport is crucial to determining the range and amount of deposition globally". The shape of microplastics are also significant in biological processes: according to Han et al. [8], "Nonspherical particles ... cylindrical polymer brushes ... and wirelike objects ... each [have] a unique influence on the cell".

By adapting off-the-shelf, low-cost hardware to build our methodology, we aim to implement our method in ecosystems in developing countries. Ecosystems in these countries are likely to experience

* Corresponding Author. Email: v$_s im@wincoll.ac.uk$

[1] Equal contribution.

high MP pollution [18], and could therefore be protected by our new methods.

2 Methodology

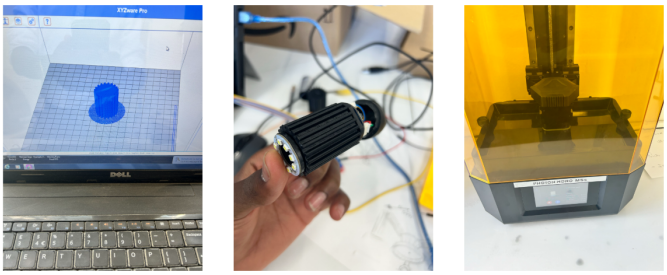

Figure 1. Images taken during the development of the focus-actuation system

Our methodology consists of two main phases: classification and point cloud generation. To collect the data necessary for inference, we built a microscope with an electronically actuated focus mechanism. We designed a custom toothed translation screw to convert the rotary motion of a 12V stepper motor to linear motion of the objective lens. This component was created via resin 3D-printing. The motor is controlled by an Arduino UNO, running the power input through a 12V relay. More details can be found in the supplementary information provided.

2.1 Classification

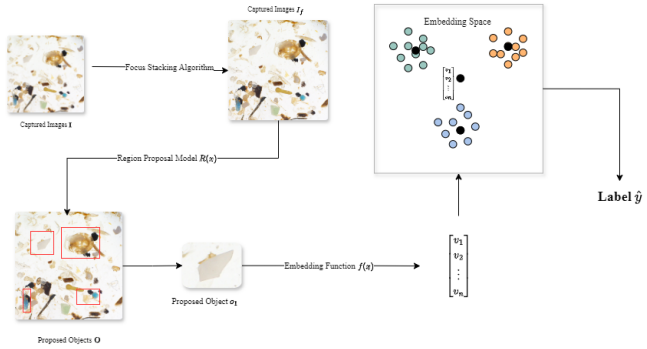

Figure 2. The classification pipeline takes images taken by the microscopes and identifies regions with microplastics.

To accurately reconstruct of objects within the scenes, the objects must first be identified. This is done with methodology proposed by Felzenszwalb et al. in "Efficient Graph-Based Image Segmentation" (EGBIS) [5]. EGBIS represents the image as a graph $G = (V, E)$, where each node $v_i \in V$ represents a pixel and each edge $(v_i, v_j) \in E$ represent similarity between pixels v_i and v_j.

The benefits of this algorithm over alternatives (e.g. YOLO [15] and CNN-based region proposal networks [17]) are twofold.

EGBIS is significantly more efficient than YOLO and CNN-based region proposal networks (RPN). The unparametised segmentation algorithm runs in $O(mlogm)$ time and runs in a fraction of a second for the 640x480 images taken by the microscope camera. YOLO and CNN-based RPNs are significantly less efficient in our application: this is as the collection of images are staggered, which means optimisations of the algorithm for GPUs are not used.

EGBIS is much more accurate than neural-network-based approaches. YOLO [15] and CNN-based RPNs [17] are trained on data that do not contain microscopy images. This means that the models are often unable to identify objects in the scene, likely as colors and structures encountered will be unfamiliar. The EGBIS algorithm does not take semantic information into account, and is thus able to identify objects despite their irregular geometries. The uniform background colour and distinct separation between adjacent particles further improve the performance of the algorithm.

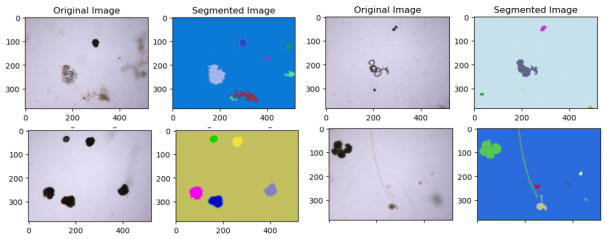

Figure 3. Example images segmented with the EGBIS algorithm. The algorithm is clearly able to identify objects in the image, regardless of the irregular structure (e.g. the fibrous structure in the bottom right image)

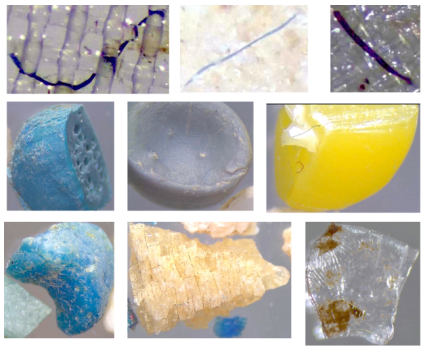

Figure 4. Microplastic Images from the ASU dataset

We perform segmentation on the model $\mathbf{M} = R(\mathbf{I}_f, k)$. The function $R(\mathbf{x}, k)$ denotes the EGBIS algorithm given the focus-stacked image $\mathbf{I}_f$ and parameter k. k parameterises the scale of objects preferred within the final segmentation (i.e. a large k will result in larger segmented objects and a smaller k will result in smaller segmented objects). The segmentation mask $\mathbf{M}$ is defined as such: the entry $\mathbf{M}_{i,j}$ denotes the object that the pixel $\mathbf{I}_f(i, j)$ is a part of. It therefore takes a value between 1 and n, where n is the number of objects.

Due to the considerable lack of light microscopy datasets, we must employ few-shot learning. For our purposes we employ a prototypical network-based methodology[16]. As proposed by Snell et al., we learn a mapping $f(x)$ from a given input image $\mathbf{x}_i$ to a point $\mathbf{c_k} \in \mathbb{R}$ in embedding space. We learn the parameters of $f(x)$ by minimising the loss function.

$$\mathcal{L} = \sum_{(\mathbf{x}_q, y_q) \in Q} \left\| f(\mathbf{x}_q) - \mathbf{c}_{y_q} \right\|^2 \tag{1}$$

where $(\mathbf{x}_q, y_q)$ is a input-label pair within the query set (the images that we aim to classify) and $\mathbf{c}_{y_q}$ is the corresponding prototype for class y_q.

We initialise our mapping $f(\mathbf{x})$ with a pretrained deep residual network [9] trained on the ImageNet dataset. We then convert the model to a mapping by replacing the final classification layer with a 512 node dense layer. Therefore, the output of the model will be the mapped point in embedding space $f(\mathbf{x}) \in \mathbb{R}^{512}$.

We fine-tune the model on the ASU MP dataset [6]. To increase the size of the MP dataset we augment the data by performing random blurring and flipping of the images. This is well motivated as the classification of a MP should be invariant to the focus and orientation of the image.

2.2 *Point Cloud Generation*

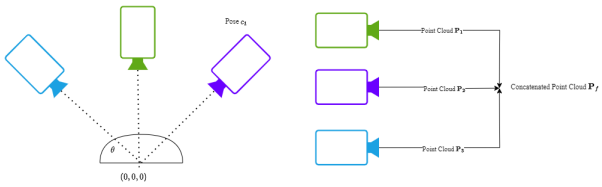

Figure 5. Collating point clouds from multiple camera perspectives

From the previous classification section, we identify the regions where a MP is present within the image. With this information, we can then continue to construct a 3D model of individual MPs. To achieve this, we employ the depth-from-focus method, an often overlooked technique.

We attempted both stereo depth estimation and monocular depth estimation but found that both methods were inadequate. For stereo depth estimation, the restrictively small field of view of microplastics makes recording images with significant parallax difficult. Similarly, monocular depth estimation is speculative when generating depth maps and is often unable to recover fine details in the image

Extracting depth information from depth-from-focus (DFF) is significantly less popular than other means due to "low precision hardware" and "imprecise mathematical methods" [21]. To make DFF an appropriate methodology for this purpose, we fix both of these limitations.

On the hardware front, our implemented solution can perform precise changes in magnification. Coupled with effective calibration, our hardware is far more effective than those used in previous implementations of DFF-based depth estimation. On the software front, we employ state-of-the-art research on blur detection to effectively extract fine details of the MPs. Specifically, we utilise Golestaneh et al.'s methodology [7] for applying blur detection on the images captured by the microscope. This is far more effective than using traditional methods (e.g. Laplacian-based methodologies) as fine details are preserved during blur detection.

We set up a camera with real coordinates $\mathbf{C}$ (using the centre of the sample as $(0, 0, 0)$) and take images with incrementing magnification and automatically disqualify images with excessively high blurriness. We also record sensor position s (the distance of the DSLR sensor from the objective lens) for each image.

For each of the images we generate a focus map $\mathbf{F}$, where $\mathbf{F}_{i,j}$ represents the focus of the pixel at (i, j). We aim to combine the focus maps generated to obtain a depth map $\mathbf{D}$ for which the entry at $\mathbf{D}_{i,j}$ denotes the distance along the ray $\mathbf{r}(t) = \mathbf{o} + t\mathbf{d}$ from $(0, 0, 0)$ and the camera position $\mathbf{C}$.

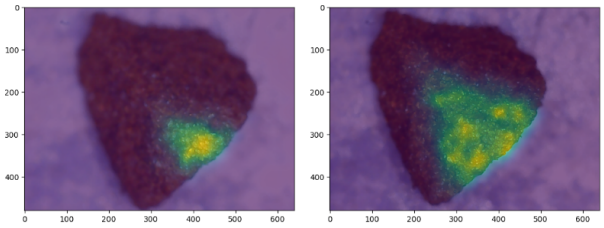

Figure 6. Example of generated focus maps of the same object and different magnifications.

The first step of this process involves aligning each of the generated focus maps, such that the focus maps can be overlaid to create an accurate depth map. This is done using the SIFT methodology [13]. Suppose we wish to align $\mathbf{F}_1$ (the focus map corresponding to $\mathbf{I}_1$) to $\mathbf{F}_2$ (the focus map corresponding to $\mathbf{I}_2$): we first generate two sets of keypoints ($\mathbf{k}_1$ and $\mathbf{k}_2$) from images $\mathbf{I}_1$ and $\mathbf{I}_2$. This is achieved by constructing a scale space and finding keypoints using a difference-of-Gaussian (DoG) function, which is applied to the image at multiple scales.

We then use a FLANN (Fast Library for Approximate Nearest Neighbors) [14] based matcher to find neighbors in $\mathbf{k}_2$ for keypoints in $\mathbf{k}_1$. Specifically, each point $k_i \in \mathbf{k}_1$ maps to some point $k_j \in \mathbf{k}_2$. We can then estimate a homography matrix $\mathbf{H}$ which best describes the mapping of the keypoints. By applying the homography matrix $\mathbf{H}$ on $\mathbf{F_1}$, we can align depth map $\mathbf{F_2}$ to $\mathbf{F}_2$. In practice, this process is highly accurate. This as the particles on screen move very slightly, making the nearest neighbor identification very accurate.

We then use this information to calculate the desired depth map $\mathbf{D}$. Using the thin-lens formula, we can trivially determine the depth of each point.

$$\mathbf{D}_{i,j} = \frac{s^* f}{s^* - f} \tag{2}$$

where f is the focal length of the camera and s^* is the sensor position that achieves maximal focus. We merge point clouds between images and With the generated point cloud, we apply Delaunay triangulation [11] to estimate the volume of the point cloud.

3 Results

We generate example meshes (Figure 7) from microplastics found during manual sample collection at the river Itchen. Training of the classification model (Table 3 and 1) is done on a GPU A100 hosted on a cloud server.

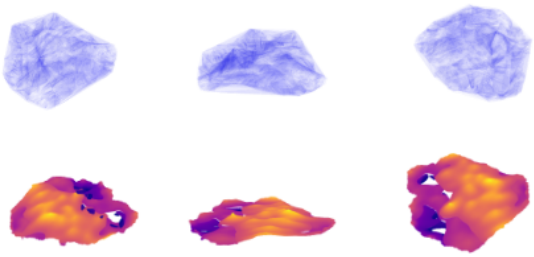

Figure 7. Top: generated mesh using images from multiple perspectives. Bottom: generated contours by placing microscope directly above microplastic.

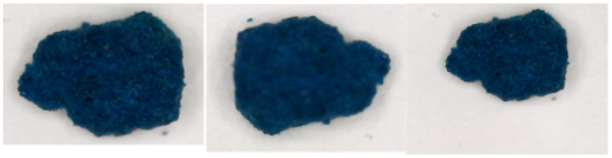

Figure 8. Example images from the top perspectives (different magnifications) that were used to construct the mesh

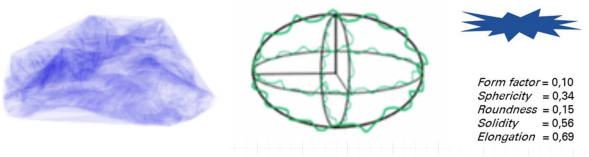

Figure 9. Comparing our methodology (left), Barchiesi model (middle), Schnepf model (right)

4 Discussion

From the results section, we can see that our classification model is highly effective in classifying MPs. With just the pretrained ResNet model, the program is able to differentiate between "bead", "fiber" and "fragment" MPs 91% of the time. When given negative samples of MPs (samples collected manually from the Itchen River and samples from other light microscopy datasets [20]), the pretrained few-shot learning model is correct 91.9% of the time. With training on the dataset, the accuracy for classification and identification both increases, but rates of false positives (i.e. identifying a MP when there is none) are still greater than that of false negatives.

The generated mesh of the MP is largely accurate, although some information is unrecoverable (e.g. the underside of the MP). Still, When tested against the original geometry, many features (e.g. prominent ridge, angularity) are preserved. This is far more effective than methodologies from Barchiesi et al. and Schnepf et al, as both are unable to fit the complex structure of the MP: Barchiesi et al assume a general elliptical structure and Schnepf et al only use 4 simple measures to define the structure of the MP. Furthermore, both cannot consider any 3D information of the MP.

Although our methodology is promising, quantitative means of evaluating the generated 3D structure will be needed to verify the model. Unfortunately, we did not have the resources to perform this analysis.

5 Conclusion

In conclusion, our methodology offers a new approach to the pressing matter of microplastic pollution. We introduce a novel solution by justifying the use of 3D analysis and present a proof-of-concept implementation of a composite classification and depth-from-focus methodology. Through efficient engineering, we even cut the cost of the solution to make it easy to implement into existing workflows. There are still issues in the methodology (e.g. inability to estimate interior of microplastic and inability for automatic sampling) but we hope that these limitations can be addressed by future papers following by this work. Supplementary information for our paper can be found on Github.

Method	Classify (%)	Identify (%)
Baseline Model (Pretrained)	91.0	91.9
Trained Model	94.6	96.3

Table 1. Comparing models before and after training on dataset. Results are on data unseen from the dataset.

Method	Identify FP (%)	Identify FN(%)
Baseline Model (Pretrained)	5.4	2.7
Trained Model	2.4	1.3

References

[1] M. Barchiesi, M. Kooi, and A. A. Koelmans. Adding depth to microplastics. *Environmental science technology*, 57(37):14015–14023, 9 2023. doi: 10.1021/acs.est.3c03620. URL https://doi.org/10.1021/acs.est.3c03620.

[2] E. Bergami, E. Bocci, M. L. Vannuccini, M. Monopoli, A. Salvati, K. A. Dawson, and I. Corsi. Nano-sized polystyrene affects feeding, behavior and physiology of brine shrimp Artemia franciscana larvae. *Ecotoxicology and environmental safety*, 123:18–25, 1 2016. doi: 10.1016/j.ecoenv.2015.09.021. URL https://doi.org/10.1016/j.ecoenv.2015.09.021.

[3] M. Bergmann, L. Gutow, and M. Klages. *Marine Anthropogenic litter*. 1 2015. doi: 10.1007/978-3-319-16510-3. URL https://doi.org/10.1007/978-3-319-16510-3.

[4] M. Eriksen, W. Cowger, L. M. Erdle, S. Coffin, P. Villarrubia-Gómez, C. J. Moore, E. J. Carpenter, R. H. Day, M. Thiel, and C. Wilcox. A growing plastic smog, now estimated to be over 170 trillion plastic particles afloat in the world's oceans—Urgent solutions required. *PloS one*, 18(3):e0281596, 3 2023. doi: 10.1371/journal.pone.0281596. URL https://doi.org/10.1371/journal.pone.0281596.

[5] P. F. Felzenszwalb and D. P. Huttenlocher. Efficient Graph-Based image segmentation. *International journal of computer vision*, 59(2):167–181, 9 2004. doi: 10.1023/b:visi.0000022288.19776.77. URL https://doi.org/10.1023/b:visi.0000022288.19776.77.

[6] U. for Data Science. Microplastics image dataset, 2021. URL https://github.com/UnitForDataScience/Microplastics_Image_Dataset. Accessed: 2024-06-25.

[7] S. A. Golestaneh and L. J. Karam. Spatially-Varying Blur Detection Based on Multiscale Fused and Sorted Transform Coefficients of Gradient Magnitudes. *CVPR*, 7 2017. doi: 10.1109/cvpr.2017.71. URL https://doi.org/10.1109/cvpr.2017.71.

[8] S. Han, J. Bang, D. Choi, J. Hwang, T. Kim, Y. Oh, Y. Hwang, J. Choi, and J. Hong. Surface pattern analysis of microplastics and their impact on Human-Derived cells. *ACS applied polymer materials*, 2(11):4541–4550, 8 2020. doi: 10.1021/acsapm.0c00645. URL https://doi.org/10.1021/acsapm.0c00645.

[9] K. He, X. Zhang, S. Ren, and J. Sun. Deep Residual Learning for Image Recognition. *CVPR 2016*, 6 2016. doi: 10.1109/cvpr.2016.90. URL https://doi.org/10.1109/cvpr.2016.90.

[10] A. A. Koelmans, N. H. M. Nor, E. Hermsen, M. Kooi, S. M. Mintenig, and J. De France. Microplastics in freshwaters and drinking water: Critical review and assessment of data quality. *Water research*, 155:410–422, 5 2019. doi: 10.1016/j.watres.2019.02.054. URL https://doi.org/10.1016/j.watres.2019.02.054.

[11] C. L. Lawson. Transforming triangulations. *Discrete mathematics*, 3(4):365–372, 1 1972. doi: 10.1016/0012-365x(72)90093-3. URL https://doi.org/10.1016/0012-365x(72)90093-3.

[12] Y. Lee, J. Cho, J. Sohn, and C. Kim. Health effects of microplastic exposures: current issues and perspectives in South Korea. *Yonsei Medical Journal/Yonsei medical journal*, 64(5):301, 1 2023. doi: 10.3349/ymj.2023.0048. URL https://doi.org/10.3349/ymj.2023.0048.

[13] T. Lindeberg. Scale invariant feature transform. *Scholarpedia journal*, 7(5):10491, 1 2012. doi: 10.4249/scholarpedia.10491. URL https://doi.org/10.4249/scholarpedia.10491.

[14] M. Muja and D. G. Lowe. Scalable nearest neighbor algorithms for high dimensional data. *IEEE transactions on pattern analysis and machine intelligence*, 36(11):2227–2240, 11 2014. doi: 10.1109/tpami.2014.2321376. URL https://doi.org/10.1109/tpami.2014.2321376.

[15] J. Redmon, S. Divvala, R. Girshick, and A. Farhadi. You Only Look Once: Unified, Real-Time Object Detection. 6 2016. doi: 10.1109/cvpr.2016.91. URL https://doi.org/10.1109/cvpr.2016.91.

[16] S. Ren, K. He, R. Girshick, and J. Sun. Prototypical networks for few-shot learning. *Conference on Neural Information Processing Systems 2017*, 2017. URL https://arxiv.org/abs/1703.05175.

[17] S. Ren, K. He, R. Girshick, and J. Sun. Faster R-CNN: Towards Real-Time Object Detection with Region Proposal Networks. *IEEE transactions on pattern analysis and machine intelligence*, 39(6):1137–1149, 6

2017. doi: 10.1109/tpami.2016.2577031. URL https://doi.org/10.1109/tpami.2016.2577031.

[18] A. T. Ta and N. Promchan. Microplastics in wastewater from developing countries: A comprehensive review and methodology suggestions. *TrAC. Trends in analytical chemistry*, 171:117537, 2 2024. doi: 10.1016/j.trac.2024.117537. URL https://doi.org/10.1016/j.trac.2024.117537.

[19] E. Ward, M. Gordon, R. Hanson, and L. M. Jantunen. Modelling the effect of shape on atmospheric microplastic transport. *Atmospheric environment*, page 120458, 3 2024. doi: 10.1016/j.atmosenv.2024.120458. URL https://doi.org/10.1016/j.atmosenv.2024.120458.

[20] E. Williams, J. Moore, S. W. Li, G. Rustici, A. Tarkowska, A. Chessel, S. Leo, B. Antal, R. K. Ferguson, U. Sarkans, A. Brazma, R. E. C. Salas, and J. R. Swedlow. Image Data Resource: a bioimage data integration and publication platform. *Nature methods*, 14(8):775–781, 6 2017. doi: 10.1038/nmeth.4326. URL https://doi.org/10.1038/nmeth.4326.

[21] Y. Xiong and S. Shafer. Depth from focusing and defocusing. *CVPR*, 12 2002. doi: 10.1109/cvpr.1993.340977. URL https://doi.org/10.1109/cvpr.1993.340977.